Fenbendazole Controls *In Vitro* Growth, Virulence Potential, and Animal Infection in the *Cryptococcus* Model

Haroldo C. de Oliveira,[a] Luna S. Joffe,[b] Karina S. Simon,[c] Rafael F. Castelli,[a] Flavia C. G. Reis,[a,d] Arielle M. Bryan,[b] Beatriz S. Borges,[a] Lia C. Soares Medeiros,[a] Anamelia L. Bocca,[c] Maurizio Del Poeta,[b,e,f] Marcio L. Rodrigues[a,g]

[a]Instituto Carlos Chagas, Fundação Oswaldo Cruz (Fiocruz), Curitiba, Brazil
[b]Department of Microbiology and Immunology, Stony Brook University, Stony Brook, New York, USA
[c]Departamento de Biologia Celular, Universidade de Brasília, Brasília, Brazil
[d]Centro de Desenvolvimento Tecnológico em Saúde (CDTS), Fundação Oswaldo Cruz, Rio de Janeiro, Brazil
[e]Veterans Affairs Medical Center, Northport, New York, USA
[f]Division of Infectious Diseases, Stony Brook University, Stony Brook, New York, USA
[g]Instituto de Microbiologia Paulo de Góes (IMPG), Universidade Federal do Rio de Janeiro, Rio de Janeiro, Brazil

Haroldo C. de Oliveira and Luna S. Joffe contributed equally to this work. Author order was determined on the basis of the future steps of the antifungal project in the Rodrigues laboratory.

ABSTRACT The human diseases caused by the fungal pathogens *Cryptococcus neoformans* and *Cryptococcus gattii* are associated with high indices of mortality and toxic and/or cost-prohibitive therapeutic protocols. The need for affordable antifungals to combat cryptococcal disease is unquestionable. Previous studies suggested benzimidazoles as promising anticryptococcal agents combining low cost and high antifungal efficacy, but their therapeutic potential has not been demonstrated so far. In this study, we investigated the antifungal potential of fenbendazole, the most effective anticryptococcal benzimidazole. Fenbendazole was inhibitory against 17 different isolates of *C. neoformans* and *C. gattii* at a low concentration. The mechanism of anticryptococcal activity of fenbendazole involved microtubule disorganization, as previously described for human parasites. In combination with fenbendazole, the concentrations of the standard antifungal amphotericin B required to control cryptococcal growth were lower than those required when this antifungal was used alone. Fenbendazole was not toxic to mammalian cells. During macrophage infection, the anticryptococcal effects of fenbendazole included inhibition of intracellular proliferation rates and reduced phagocytic escape through vomocytosis. Fenbendazole deeply affected the cryptococcal capsule. In a mouse model of cryptococcosis, the efficacy of fenbendazole to control animal mortality was similar to that observed for amphotericin B. These results indicate that fenbendazole is a promising candidate for the future development of an efficient and affordable therapeutic tool to combat cryptococcosis.

KEYWORDS *Cryptococcus*, antifungal, fenbendazole

Cryptococcosis caused by *Cryptococcus neoformans* and *Cryptococcus gattii* kills almost 200,000 humans each year (1). The disease, which is devastating in sub-Saharan Africa, significantly affects other regions of the globe, including Asia, Oceania, Europe, and the Americas (2–4). The World Health Organization (WHO) recently recommended three therapeutic phases for treating cryptococcal meningitis, including an induction therapy with amphotericin B plus flucytosine (week 1) followed by fluconazole (week 2), a consolidation phase with fluconazole (weeks 3 to 10) and maintenance therapy of up to 12 months also with fluconazole (5, 6). However, amphotericin B and flucytosine are not available in many countries (7). In addition, the effective treatment

of human cryptococcosis is cost prohibitive in most of the regions that are severely affected by *C. neoformans* and *C. gattii* (8). In Brazil, the therapeutic costs of lipid formulations of amphotericin B can exceed $100,000 per patient (9). In summary, novel therapeutic protocols for treating the diseases caused by *C. neoformans* and *C. gattii* are urgent. However, the development of novel drugs is time-consuming, highly expensive, and commonly unsuccessful (10, 11). In this context, drug repurposing has emerged as a promising alternative for the development of novel therapies against neglected pathogens, including fungi (12–14).

Benzimidazoles are anthelmintic compounds that were introduced in clinical practice nearly 60 years ago (15). *C. neoformans* and *C. gattii* are sensitive to benzimidazoles *in vitro* (16–18). Flubendazole is inhibitory against all pathogenic *Cryptococcus* species, including isolates that are resistant to fluconazole (14). In mice, orally administered flubendazole resulted in a reduction in fungal burden in comparison with controls, but in the rabbit model, there were no quantifiable drug concentrations or antifungal activity in the cerebrospinal fluid or brain (19). Mebendazole, another member of the family of benzimidazoles, also showed antifungal activity against *C. neoformans*, including phagocytized yeast cells and cryptococcal biofilms (20).

The anticryptococcal effects of other benzimidazoles have been superficially examined. In comparison to other benzimidazoles, fenbendazole was the most efficient compound showing *in vitro* fungicidal activity (20), but mechanistic approaches and *in vivo* activity of this compound were not evaluated. Fenbendazole has been licensed worldwide for the treatment and control of helminth infections in food-producing and non-food-producing animals for more than 30 years, and its safety is well established. According to the European Medicines Agency (21), fenbendazole had negligible acute toxicity in single-dose animal studies, and no points of concern relevant for the safety of fenbendazole in humans could be identified, although the effects of multiple doses are still not known. No treatment-related effects were observed in the offspring of dogs, pigs, sheep, and cattle administered fenbendazole at various times during gestation. Finally, the compound was not genotoxic, and no evidence of carcinogenicity was found (21, 22).

Based on the anticryptococcal effects of fenbendazole (20) and negligible toxicity to humans and animals (21, 22), we evaluated the therapeutic potential of this benzimidazole against pathogenic cryptococci. Our results demonstrated that fenbendazole was inhibitory against several strains of *C. neoformans* and *C. gattii*. The mechanism of antifungal activity of fenbendazole involved the functionality of microtubules. Fenbendazole had low toxicity to mammalian cells alone or in combination with amphotericin B, and its antifungal effects included inhibition of virulence determinants and reduced proliferation of *Cryptococcus* inside macrophages. Finally, fenbendazole was highly effective in a mouse model of cryptococcosis. These results support the use of fenbendazole as a prototype for the development of novel pharmaceutical preparations for treating cryptococcosis.

RESULTS

Fenbendazole affects several isolates of *Cryptococcus* and has low toxicity to mammalian cells. We first determined the MIC of fenbendazole against strains H99 and R265, the standard isolates of *C. neoformans* and *C. gattii*, respectively. A similar MIC of 0.012 μg/ml was found for both strains (Fig. 1A). We tested 12 additional isolates of *C. neoformans* and 3 other isolates of *C. gattii*, and the same MIC of 0.012 μg/ml was found for all of them, despite their differential susceptibility to fluconazole and amphotericin B (Table 1). At the MIC, fenbendazole exerted fungicidal effects, as concluded from the highly reduced detection of CFU of *C. neoformans* and *C. gattii* after exposure to the drug (Fig. 1B). In a toxicity model using mammalian macrophages, the concentration of fenbendazole required to kill 50% of the cell population (LD_{50}) corresponded to 3.072, generating a selectivity index (LD_{50}/MIC) of 256. This result confirmed the low toxicity of fenbendazole.
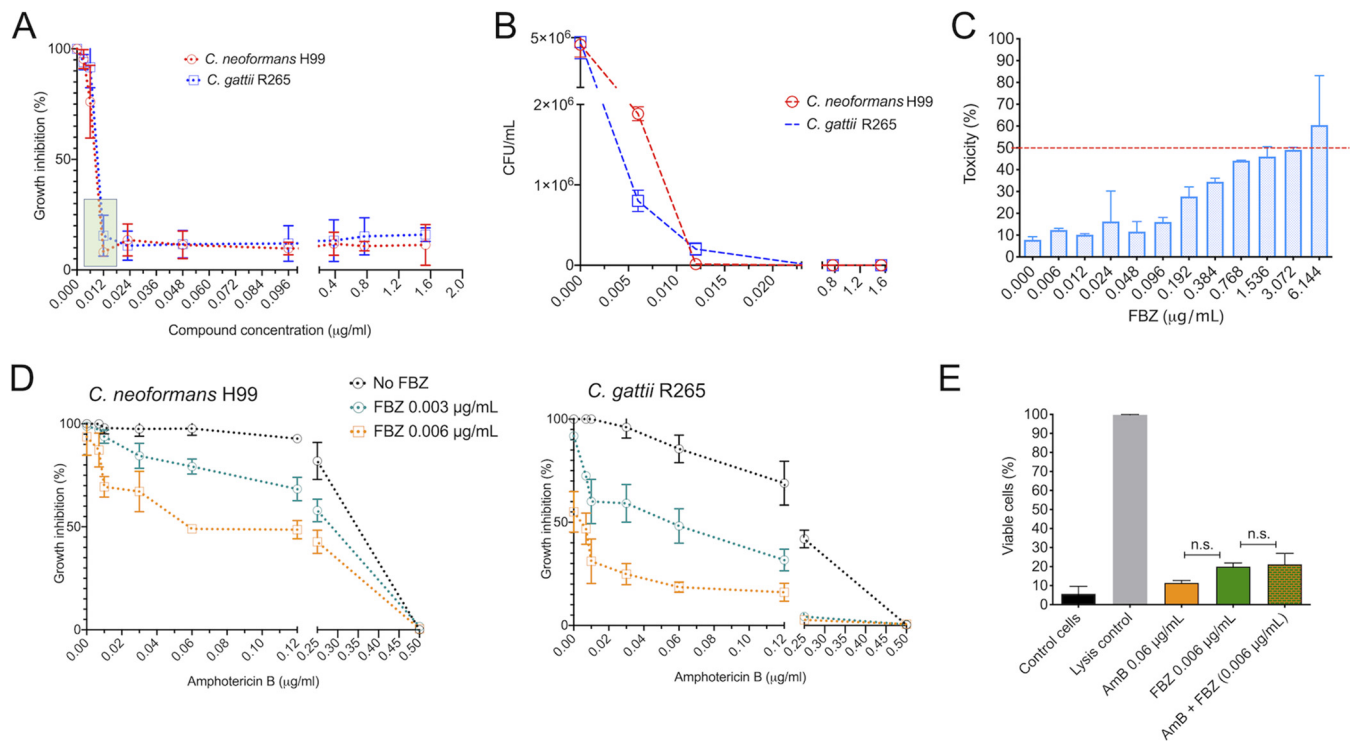
FIG 1 Antifungal effect and toxicity of fenbendazole (FBZ). (A) Determination of the MIC of fenbendazole against *C. neoformans* (strain H99) and *C. gattii* (strain R265). Both strains were sensitive to a MIC of 0.012 μg/ml (boxed area). (B) FBZ is fungicidal, as concluded from its ability to drastically reduce the numbers of CFU of *C. neoformans* H99 and *C. gattii* R265 at the MIC. (C) Dose-dependent profile of toxicity of fenbendazole against RAW 264.7 macrophages. The dotted line represents the 50% cutoff of cellular viability. (D) Antifungal effects of subinhibitory doses of fenbendazole (0.003 and 0.006 μg/ml) in combination with variable concentrations of amphotericin B (AmB) against *C. neoformans* H99 and *C. gattii* R265. In both cases, the presence of fenbendazole results in decreased concentrations of amphotericin B required for growth inhibition. (E) Analysis of the potential of fenbendazole and amphotericin B alone or in combination to kill RAW 264.7 macrophages. Control cells consisted of mammalian cultures treated with vehicle (DMSO) alone. Lysis control consisted of cells treated with 1× lysis solution (provided by the manufacturer). No significant (n.s.) differences were found between the antifungal preparations.

Fenbendazole potentiated the antifungal activity of amphotericin B, as inferred from the results obtained from the checkerboard assay. When used alone, amphotericin B produced a MIC of 0.5 μg/ml against both *C. neoformans* (H99 strain) and *C. gattii* (R265 strain). However, when tested in combination with 0.006 μg/ml fenbendazole, the amphotericin B MIC was decreased 8-fold (0.06 μg/ml). Indeed, dose-response analyses efficiently illustrate that the anticryptococcal effects of amphotericin B are boosted by different concentrations of fenbendazole, especially against *C. gattii* R265 (Fig. 1D). Analysis of the toxic effects of the compounds in combination or alone revealed that all systems had low and similar toxicity to mammalian macrophages (Fig. 1E).

The fractional inhibitory concentration index (FICI) corresponded to 0.62 for *C. neoformans* H99 and 0.49 for *C. gattii* R265. These data suggested that the combination was synergistic only in the *C. gattii* R265 isolate. However, considering that fenbendazole and amphotericin B belong to different molecular classes with distinct cellular targets, we also evaluated our synergism data using the SynergyFinder tool (https://synergyfinder.fimm.fi) applying the Bliss independence model, which is based on stochastic processes in which two drugs elicit their effects independently (23). With this method, scores of less than −10 indicate that the interaction between two drugs is antagonistic. Scores from −10 to 10 suggest an additive effect, and scores larger than 10 indicate synergism. For *C. neoformans* H99, the average Bliss synergy score considering all concentrations tested corresponded to 4.755 (Fig. 2A). In *C. gattii* R265, we obtained an average score of 5.225 (Fig. 2B). However, the analysis of synergism focused on specific concentration ranges produced more promising scores. For *C. neoformans* H99, for instance, a highly synergistic score of 42.14 was calculated when amphotericin B and fenbendazole were used at 0.025 and 0.006 μg/ml, respectively. A

TABLE 1 Determination of MICs in different isolates of *C. neoformans* and *C. gattii* using fenbendazole (FBZ), fluconazole (FCZ), and amphotericin B as antifungals[a]

Isolate[b]	Origin	MIC (µg/ml) for:		
		FBZ	FCZ	AmB
C. neoformans H99	Clinical	0.012	2.0	0.5
C. neoformans 162	Clinical	0.012	8.0	0.5
C. neoformans 191	Clinical	0.012	8.0	0.25
C. neoformans 186	Clinical	0.012	4.0	0.25
C. neoformans 161	Clinical	0.012	4.0	0.5
C. neoformans 160	Clinical	0.012	4.0	0.5
C. neoformans 139	Clinical	0.012	4.0	0.5
C. neoformans 118	Clinical	0.012	8.0	0.25
C. neoformans 116	Clinical	0.012	8.0	0.5
C. neoformans 115	Clinical	0.012	4.0	0.5
C. neoformans 222	Clinical	0.012	2.0	0.5
C. neoformans 223	Clinical	0.012	4.0	0.5
C. neoformans 218	Clinical	0.012	2.0	0.25
C. gattii R265	Clinical	0.012	8.0	0.5
C. gattii 367	Environmental	0.012	8.0	0.25
C. gattii 368	Environmental	0.012	16.0	0.25
C. gattii 365	Environmental	0.012	4.0	0.5
C. krusei ATCC 6258[c]	Not applicable	>1.536	>64	0.25
C. parapsilosis ATCC 22019[c]	Not applicable	>1.536	1.0	0.25

[a]As determined by EUCAST, growth inhibition measurements corresponded to 50% for FLZ and 90% for AmB. FBZ inhibition rates shown in the table correspond to 90%. Identical values were obtained when 50% inhibition rates were determined for FBZ (data not shown).
[b]Strain numbers were attributed by the Collection of Pathogenic Fungi of Fiocruz. For details, see http://cfp .fiocruz.br/index.
[3]The *C. krusei* and *C. parapsilosis* isolates were used as controls of antifungal activity as preconized by EUCAST. The MIC results obtained with these isolates were at the expected range (47).

similar analysis with *C. gattii* R265 generated a score of 43.13 when amphotericin B and fenbendazole were used at 0.1250 and 0.003 µg/ml, respectively. The synergistic activity was observed in an even broader concentration interval. In the combined concentration range of 0.003 to 0.006 µg/ml of fenbendazole and 0.06 to 0.25 µg/ml of amphotericin B, Bliss scores of 20.08 and 20.56 were calculated for *C.*
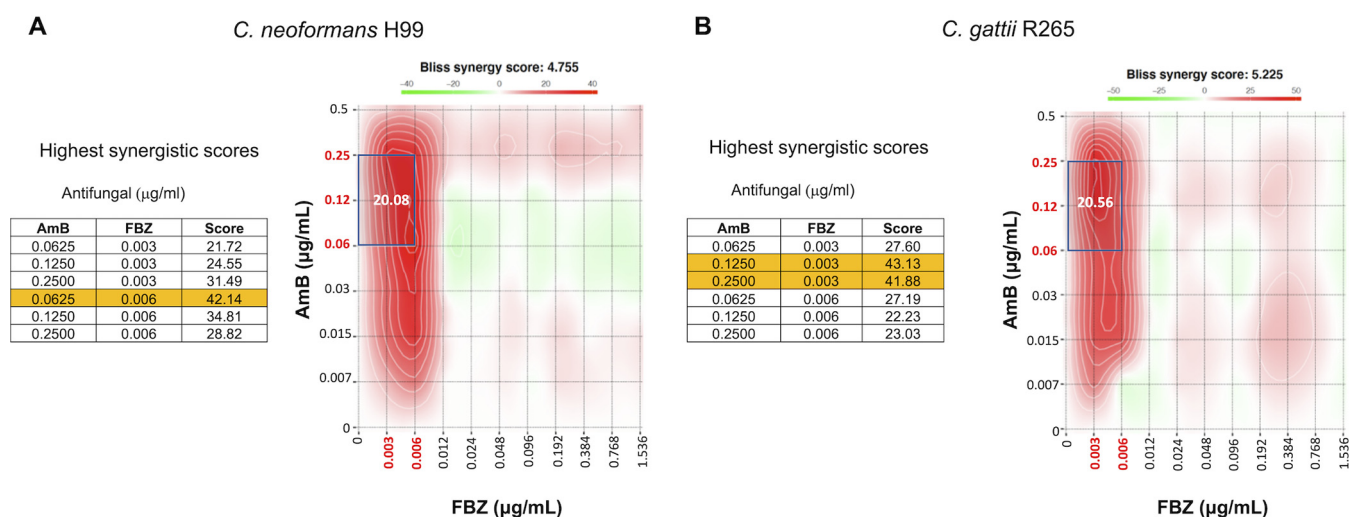

FIG 2 Synergistic antifungal activity of fenbendazole (FBZ) and amphotericin B (AmB) against *C. neoformans* H99 (A) and *C. gattii* R265 (B). The average Bliss synergy scores calculated using the full concentration range of each compound in the checkerboard assay corresponded to 4.755 and 5.225 for isolates H99 and R265, respectively. However, calculations using the antifungal concentrations producing the highest synergistic scores (left panels in A and B) generated Bliss scores of 20.08 and 20.56 for *C. neoformans* H99 and *C. gattii* R265, respectively (boxed areas in the heatmap plots). Yellow rows correspond to the highest Bliss scores obtained in our analysis. For data interpretation, please consider Bliss score values of less than –10 for antagonistic compounds, –10 to 10 for an additive effect, and larger than 10 for synergism. Calculations and graphical presentations were obtained with the SynergyFinder tool (https://synergyfinder.fimm.fi).
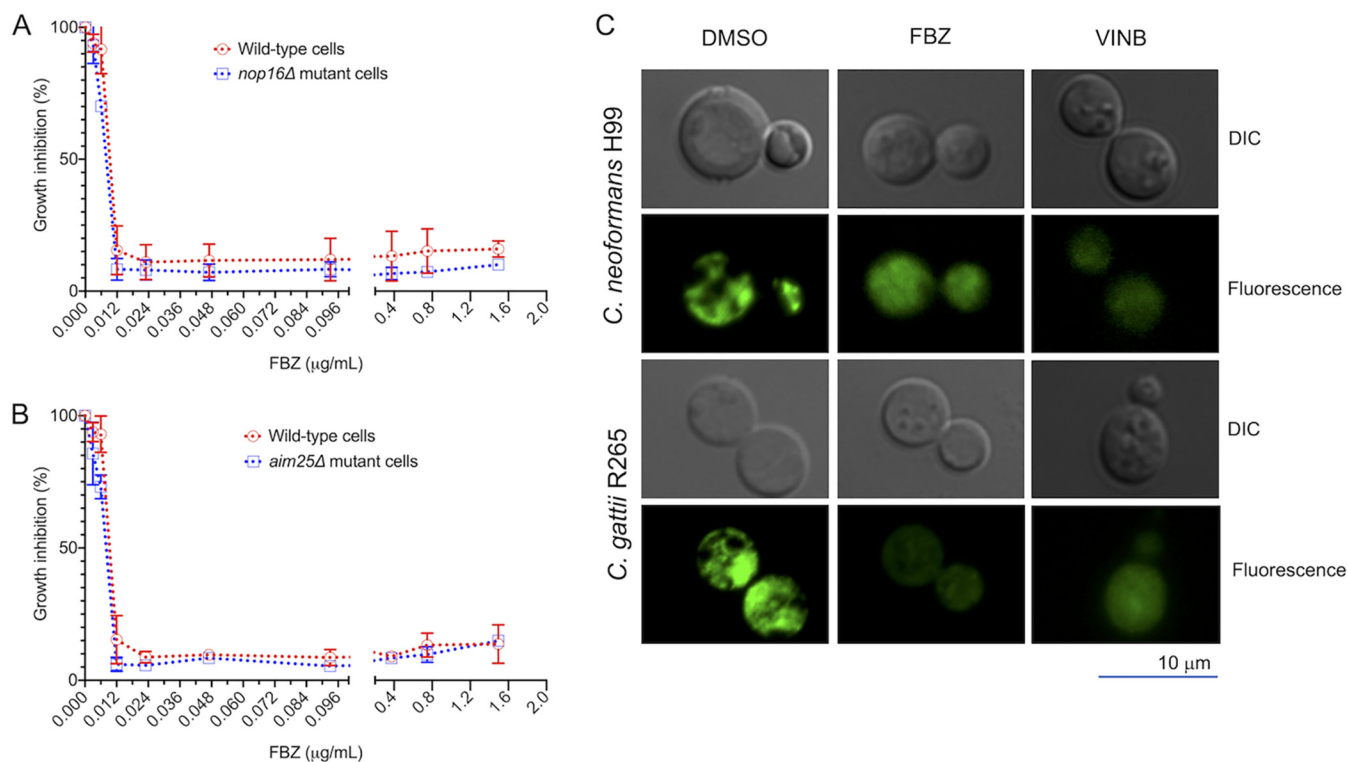
FIG 3 The antifungal effects of fenbendazole are related to microtubule disorganization. Nop16 and Aim25, which were previously suggested to be the targets of the antifungal activity of benzimidazoles in *C. gattii*, are not involved in the antifungal activity of fenbendazole (FBZ), as concluded from the similar growth rates observed for wild-type *C. gattii* (R265 strain) and mutant cells lacking *NOP16* (A) or *AIM25* (B) in the presence of variable concentrations of FBZ. A comparison between the β-tubulin staining pattern in control cells (DMSO) and FBZ-treated fungi (C) revealed that drug treatment profoundly affected microtubule distribution, with apparently more intensive effects on *C. gattii* R265. Similar staining patterns were obtained when both strains were treated with vinblastine. Fungal cells are shown under the differential interference contrast (DIC) and fluorescence modes.

neoformans H99 and *C. gattii* R265, respectively. These results indicate that fenbendazole and amphotericin B have synergistic activity against the two standard isolates of *Cryptococcus* used in our study.

Fenbendazole affects β-tubulin distribution in *C. neoformans* and *C. gattii*. We asked whether the mechanism of anticryptococcal activity of fenbendazole was similar to what was previously described for *C. gattii* (20) or if it was related to its well-characterized anthelmintic effect (15, 24, 25). Mutant strains of *C. gattii* lacking expression of the Aim25 scramblase or the nucleolar protein Nop16 were resistant to mebendazole (20), suggesting that these proteins are potential targets for the antifungal activity of benzimidazoles. To investigate the mechanism of action of fenbendazole, we first evaluated its antifungal activity against mutant strains of *C. gattii* lacking the *AIM25* or *NOP16* genes and observed that both strains and wild-type cells were similarly sensitive to this benzimidazole (Fig. 3A and B). This result suggested that, in contrast to mebendazole, Aim25 and Nop16 are not required for the antifungal activity of fenbendazole. We then asked whether the inhibitory effect of fenbendazole against *C. neoformans* H99 and *C. gattii* R265 involves interference with the functions of β-tubulin, as is consistently described for parasites (15, 24). Staining of β-tubulin in fungal cells revealed that drug-treated fungi and untreated cryptococci had markedly different profiles of microtubule organization. Control cells showed high fluorescence intensity and a well-defined intracellular pattern of β-tubulin staining (Fig. 3C). Fluorescence detection was apparently less intense in fenbendazole-treated cells, which also manifested a markedly more disperse staining of β-tubulin. In addition, the effects of fenbendazole on β-tubulin staining were apparently more drastic in *C. gattii* R265 than in *C. neoformans* H99, as concluded from the weaker signals of β-tubulin staining in the former species. These results were similar to those obtained with the control drug
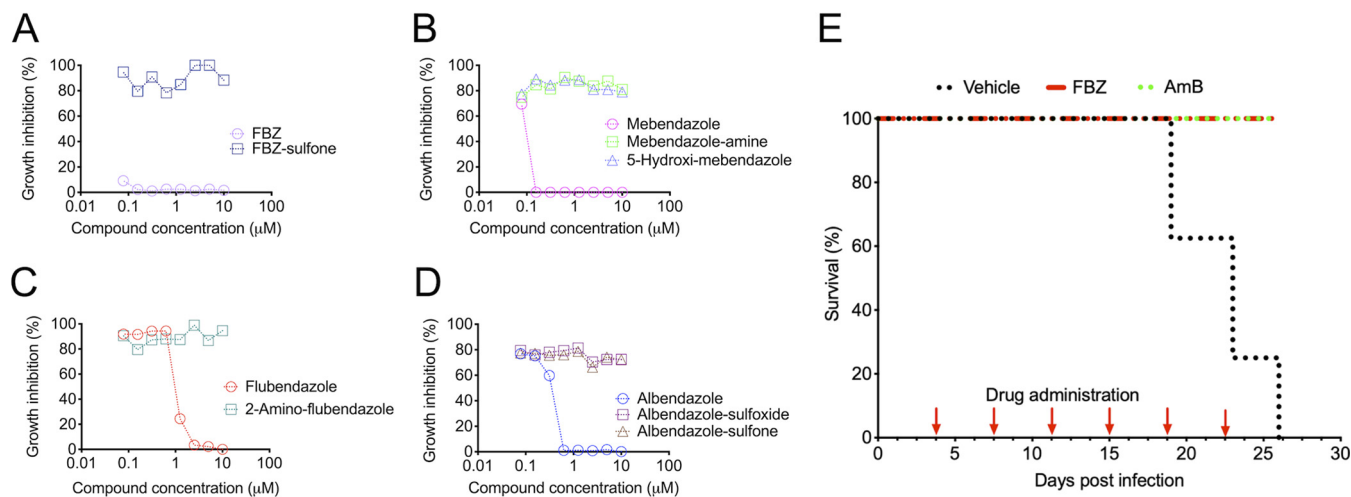
FIG 4 Analysis of the potential of fenbendazole to control animal cryptococcosis. (A to D) Antifungal effects of fenbendazole and other benzimidazoles in comparison with their liver metabolites. All benzimidazoles had clear antifungal activity, in contrast to their liver metabolites of fenbendazole (A), mebendazole (B), flubendazole (C), and albendazole (D). (E) Treatment of lethally infected mice with intranasally delivered fenbendazole or intraperitoneally administered amphotericin B (AmB). All vehicle-treated animals died 26 days postinfection. Drug-treated animals were all alive 27 days postinfection.

vinblastine, which binds tubulin and inhibits the assembly of microtubules (26), indicating that the mechanism of antifungal activity of fenbendazole against *Cryptococcus* is similar to that described for human parasites.

Intranasal administration of fenbendazole results in the control of animal cryptococcosis. The combination of low toxicity, antifungal efficacy, and a defined mechanism of action led us to test the antifungal potential of fenbendazole *in vivo*. To keep the number of animals used to a minimum, we selected the standard strain H99 of *C. neoformans* for the *in vivo* work, based on the highest prevalence of this species in human disease (3). Metabolization by host tissues is a common feature of orally administered benzimidazoles (27). Fenbendazole, specifically, is rapidly sulfoxidated by liver microsomes after oral absorption (27). Therefore, using *C. neoformans* H99, we first tested the *in vitro* antifungal activity of the sulfone derivative of fenbendazole, which showed no inhibitory potential (Fig. 4A). We performed similar tests with the liver metabolites of other benzimidazoles (mebendazole, flubendazole, and albendazole), and none of them manifested antifungal activity (Fig. 4B to D), suggesting that host metabolization is an important limitation for the antifungal activity of benzimidazoles in general. In fact, orally administered fenbendazole and mebendazole had no effects on mouse cryptococcosis (see Fig. S1 in the supplemental material). Therefore, to avoid liver metabolization and to promote an increased bioavailability of fenbendazole in its native form, we administered the drug intranasally. Under these conditions, mice lethally infected with *C. neoformans* H99 receiving intraperitoneal amphotericin B and intranasal fenbendazole had similarly high survival rates in comparison with vehicle-treated mice ($P = 0.0014$; Fig. 4E). The experiment was repeated under the same conditions, and identical results were obtained.

Fenbendazole affects the virulence potential of *Cryptococcus*. We asked whether the high efficacy of fenbendazole *in vivo* was related to neutralization of virulence determinants in addition to its antifungal effects. Capsule synthesis and intracellular proliferation rates have been consistently associated with the pathogenic potential of cryptococci (28, 29). We therefore evaluated whether fenbendazole was able to interfere with each of these biological events.

Microscopic analysis of fenbendazole-treated *C. neoformans* H99 and *C. gattii* R265 revealed clear effects on the capsular architecture, although some strain-specific particularities were observed. In all cases, fungal aggregates with reduced capsular dimensions were observed after drug treatment (Fig. 5A). Scanning electron microscopy of the H99 strain of *C. neoformans* after exposure to fenbendazole revealed shorter and
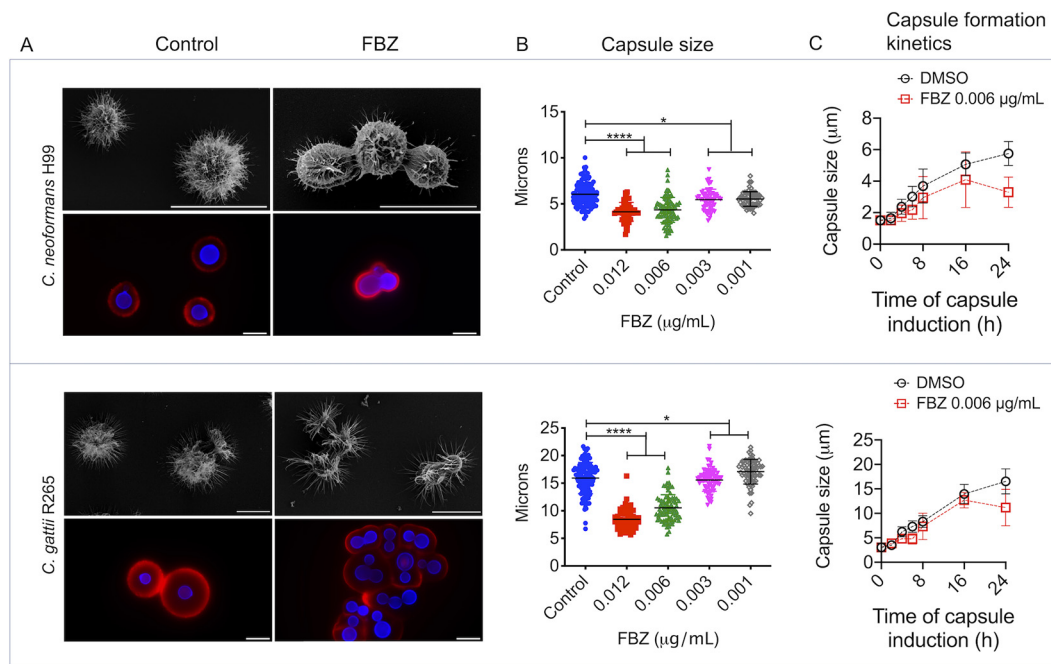
FIG 5 Fenbendazole (FBZ) affects capsule formation in *C. neoformans* and *C. gattii*. (A) Morphological analysis of vehicle (control) and drug-tread *C. neoformans* (strain H99) and *C. gattii* (strain R265). For each species, the top panels illustrate capsular alterations with scanning electron microscopy, and the bottom panels illustrate capsular morphology (red fluorescence) and cell wall staining (blue fluorescence). Scale bars, 10 μm. (B) Quantitative determination of capsular dimensions after treatment of fungal cells with vehicle alone (control) or variable concentrations of fenbendazole. *, $P < 0.05$; ****, $P < 0.0001$. (C) Kinetics of capsule formation in *C. neoformans* H99 and *C. gattii* R265 in the presence or absence of fenbendazole. The inhibitory effect on capsule formation was evident after 24 h of exposure to the drug.

scarcer capsular fibers than control cells. This perception was confirmed using immunofluorescence analysis. In *C. gattii* (strain R265), surface fibers and capsular dimensions were also reduced after exposure to fenbendazole. In both cases, a dose-dependent reduction of capsular dimensions was observed after cryptococci were treated with fenbendazole (Fig. 5B). For both *C. neoformans* H99 and *C. gattii* R265, the inhibitory effect on capsule formation was evident after 24 h of exposure to the drug, as concluded from a comparative time course analysis of capsule formation in the absence or presence of fenbendazole (Fig. 5C).

Due to the suggested link between therapeutic failure and intracellular proliferation of cryptococci (28, 30, 31), we evaluated whether fenbendazole could influence the fate of *C. neoformans* H99 and *C. gattii* R265 in infected macrophages. Initial microscopic observation suggested that fenbendazole affected the cell division frequency of both *C. neoformans* H99 and *C. gattii* R265 (Fig. 6A and B). In macrophages infected with *C. neoformans* H99 that were further treated with dimethyl sulfoxide (DMSO), intracellular division was initially observed 1 h after internalization of fungal cells, with a clear peak at 5 h postphagocytosis (Fig. 6C). In drug-treated systems, intracellular proliferation was first observed 4 h after phagocytosis, with less intense peaks at 5 and 7 h postinfection. In similar systems using *C. gattii* R265, intracellular proliferation in vehicle-treated macrophages was first observed 1 h postinfection, with more prominent peaks of replication at 5 and 7 h postinfection (Fig. 6D). In drug-treated systems, fungal intracellular proliferation was only observed after 5 h. These results were suggestive of lower intracellular proliferation rates (IPR) of phagocytized *C. neoformans* H99 and *C. gattii* R265. Since low IPR have been linked with reduced virulence (28, 30, 32), we investigated the effects of fenbendazole on this important parameter.

In both species, exposure of infected macrophages to fenbendazole resulted in reduced IPR at both inhibitory and subinhibitory concentrations (Fig. 7A and B). High IPR are related to vomocytosis, a mechanism of phagocytic escape commonly used by
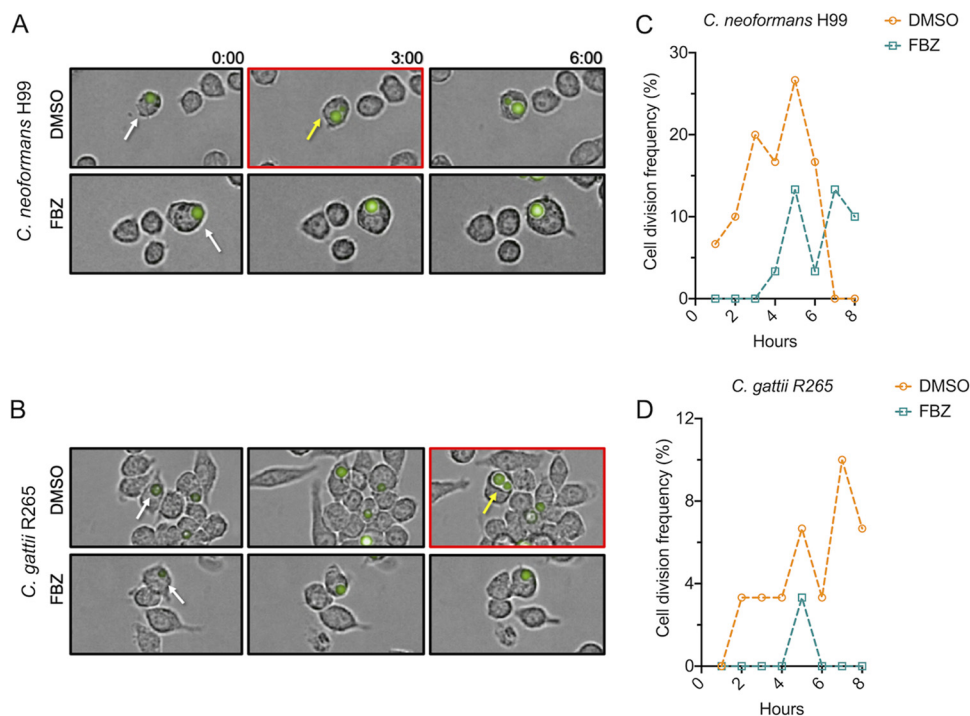
FIG 6 Time-lapse detection of budding yeast cells in macrophages infected with *C. neoformans* (strain H99) or *C. gattii* (strain R265). Video-microscopy analysis of macrophages infected with single-cell *C. neoformans* (A) or *C. gattii* (B) (white arrows) suggested that detection of yeast budding (yellow arrows) is delayed in fenbendazole (FBZ)-treated systems in comparison with vehicle (DMSO)-treated macrophages. Panels boxed in red denote the initial detection of yeast budding. This initial perception was confirmed by a quantitative analysis of intracellular budding for *C. neoformans* (C) and *C. gattii* (D).

Cryptococcus (33, 34). We therefore determined the vomocytosis levels after exposure of infected macrophages to fenbendazole. Similarly, fenbendazole reduced the rates of vomocytosis at both inhibitory and subinhibitory concentrations in macrophages infected with *C. neoformans* H99 or *C. gattii* R265 (Fig. 6C and D). Since IPR and vomocytosis are directly linked to the ability of *Cryptococcus* to survive after ingestion by phagocytic cells, we also counted viable CFU of *C. neoformans* H99 and *C. gattii* R265 after interaction with the macrophages. Once again, treatment of the mammalian cells with fenbendazole affected the growth of *C. neoformans* H99 and *C. gattii* R265. In both cases, CFU counts were reduced after treatment of infected cells with fenbendazole (Fig. 7E and F). Once again, fenbendazole promoted an increase in the antifungal efficacy of amphotericin B, as inferred from the reduced concentration of this antifungal required for the intracellular killing of *C. neoformans* H99 and *C. gattii* R265 (Fig. 7E and F).

DISCUSSION

The *in vitro* anticryptococcal activity of benzimidazoles has been consistently reported (14, 16, 19, 20). A general analysis of these reports indicated that, among all members of this drug family, fenbendazole required the lowest MIC against *C. neoformans* and *C. gattii* in comparison to other benzimidazoles (14, 16, 19, 20). In addition, a detailed study of the toxicity of fenbendazole suggested high levels of safety in humans (21, 22), which contrasts with the high toxicity of amphotericin B (35). In our study, we confirmed the efficacy of fenbendazole as an anticryptococcal agent. We tested 17 strains of *C. neoformans* and *C. gattii* and observed that they were all similarly susceptible to fenbendazole, suggesting that intrinsic resistance to this benzimidazole may not be a problem with this drug. A similar MIC of 0.012 μg/ml was found for all of them. For comparison, a recent study (19) analyzed 50 strains of *C. neoformans* according to their susceptibility to flubendazole, another member of the benzimidazole
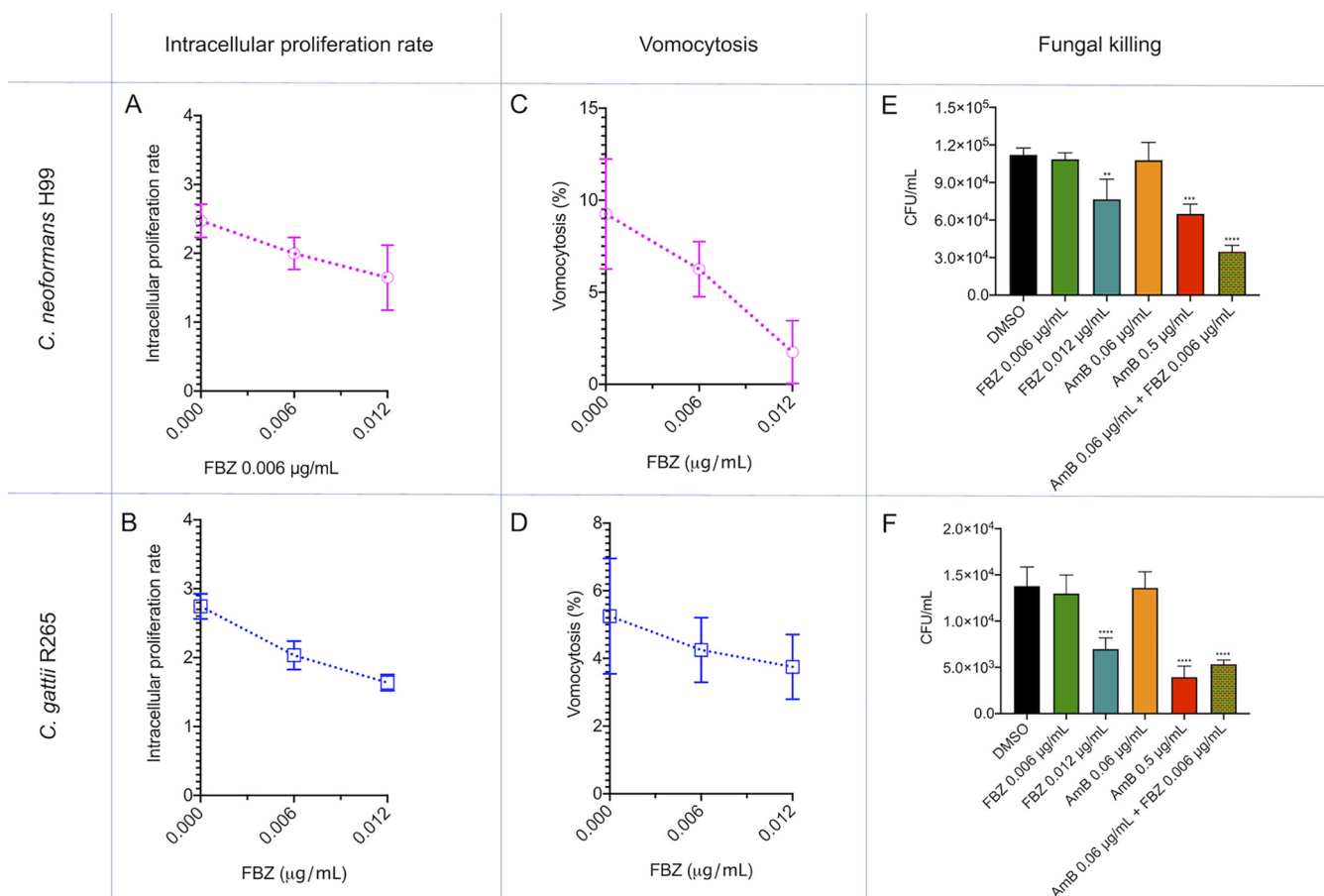
FIG 7 Effects of fenbendazole (FBZ) on the intracellular fate of *Cryptococcus*. Treatment with fenbendazole decreased the intracellular proliferation rates of *C. neoformans* (strain H99) (A) and *C. gattii* (strain R265) (B). Similar profiles of inhibitory effects were observed when vomocytosis was analyzed in macrophages infected with *C. neoformans* (C) or *C. gattii* (D). The recovery of significantly fewer fungal cells from FBZ-treated macrophages (0.012 μg/ml) indicated intracellular activity against *C. neoformans* H99 (E) and *C. gattii* R265 (F). Similar results were obtained with an antifungal concentration range of amphotericin B (AmB) or with a combination of subinhibitory doses of AmB and FBZ. **, $P = 0.01$; ***, $P = 0.001$; ****, $P < 0.0001$.

family. Using the same EUCAST methodology, MICs of 0.03 (one strain), 0.06 (19 strains), 0.125 (25 strains), and 0.25 (5 strains) μg/ml were found in this study. These values were 2.5- to 20-fold higher than the MIC found for fenbendazole in this study. The low toxicity of fenbendazole was also confirmed in our experimental model, as well as its ability to improve the antifungal activity of amphotericin B. In earlier studies, it was demonstrated that concentration of fenbendazole required to kill *Cryptococcus* was 8.5-fold lower than that of amphotericin B (16). These characteristics led us to explore the properties of fenbendazole in mechanistic and therapeutic models.

In a previous study, we used a mutant collection of *C. gattii* for determination of the cellular targets of mebendazole, another anticryptococcal benzimidazole (20). These mutants were screened for resistance phenotypes in the presence of mebendazole based on the assumption that in the absence of a cellular target required for antifungal activity, the drug would lack anticryptococcal properties. The mutants showing the highest levels of resistance to mebendazole lacked expression of Aim25, a cryptococcal scramblase (36), or Nop16, a putative nucleolar protein (20). We initially assumed that these targets were required for the activity of fenbendazole, but our current results indicate that they are not involved in the antifungal properties of this benzimidazole. In nematodes, the benzimidazoles bind to β-tubulin, leading to local unfolding of the protein and consequent abnormal conformation. This outcome results in the inhibition of the polymerization of α- and β-tubulin subunits to form microtubules, causing lethal effects in dividing cells (37). In the *C. neoformans* model, a similar mechanism was

attributed to flubendazole and other benzimidazoles (38). However, fenbendazole was not specifically tested in these studies. In addition, the cellular effects of benzimidazoles on the cryptococcal microtubules were not reported. In our study, treatment of both *C. neoformans* and *C. gattii* with fenbendazole led to a clear alteration in β-tubulin detection, strongly suggesting that its mechanism of action is related to that described for the nematodes and other parasites.

The benzimidazoles are extensively metabolized in mammals following oral administration. The parent compounds are generally short-lived, and metabolites predominate in plasma, tissues, and excreta (27). Fenbendazole, for instance, is rapidly metabolized by liver microsomes after oral absorption. In pigs, this benzimidazole was rapidly absorbed after oral administration, but its systemic bioavailability was low (39). The intranasal route, on the other hand, transports drugs directly to the brain from the nasal cavity along the olfactory and trigeminal nerves (40), avoiding the first-pass metabolism in the liver and gastrointestinal tract. Another advantage of the intranasal route of drug delivery is the rapid absorption of bioactive compounds. For instance, midazolam, a benzodiazepine depressant, reaches clinically effective concentrations within less than 10 min after nasal administration in humans (41). The low molecular mass of fenbendazole (299.349 g/mol) also favors brain absorption after intranasal administration (42). These findings agree with our current results showing that all animals infected with *C. neoformans* and treated with fenbendazole intranasally survived. However, our results also suggest that liver metabolization is a limitation for the oral treatment of fungal diseases with fenbendazole. In this sense, strategies for protecting drug candidates against metabolic modifications are widely available (43), and they could be applied to the use of fenbendazole as a scaffold for antifungal development. Most likely, intranasal pharmaceutical preparations of fenbendazole could be promising and safe therapeutic alternatives in the *Cryptococcus* model.

Interference with pathogenic traits in addition to primary antifungal effects were likely related to the high efficacy of fenbendazole in the control of animal cryptococcosis observed in our study. High levels of uptake of cryptococci by macrophages *in vitro* have been associated with long-term survival of human patients (44). Importantly, strains showing high uptake by macrophages were hypocapsular. The connections between phagocytic events, reduced capsules, and the outcome of human disease formed the basis of our studies on the effects of fenbendazole on capsular architecture and outcome of macrophage infection. Fenbendazole produced effects that are potentially positive to the host in all cases, since it caused a decrease in capsular density and dimensions, in addition to reducing intracellular proliferation rates and events required for phagocytic escape.

It was estimated that the cost to procure one million doses of standard benzimidazoles (500 mg each) would be approximately $20,000, including international transport (45). In comparison to the cost of treating cryptococcosis patients with lipid formulations of amphotericin B (9, 10), these numbers are extraordinarily low. In this context, our results support the development of pharmaceutical preparations of fenbendazole to be tested as alternative anticryptococcal agents. If effective in humans, fenbendazole could represent an affordable alternative for the treatment of a disease that has an extremely negative impact on the health conditions of neglected populations.

MATERIALS AND METHODS

Strains and growth conditions. *Cryptococcus neoformans* and *C. gattii* (strains H99 and R265, respectively) were used in most experiments. Of note, the reference strain R265 has been recently reclassified as *C. deuterogattii*. In this study, we kept its classification as *C. gattii*, as largely employed in the *Cryptococcus* literature. In addition, 12 isolates of *C. neoformans* (VNI genotype) and 3 isolates of *C. gattii* (VGI genotype), obtained from the Collection of Pathogenic Fungi available at the Oswaldo Cruz Foundation (Fiocruz), were tested for susceptibility to fenbendazole. For studies of mechanisms of antifungal activity, the *C. gattii* mutant strains *aim25Δ* and *nop16Δ* were also tested (20, 36). For the *in vitro* interaction assays, green fluorescence protein (GFP)-tagged *C. neoformans* and *C. gattii* were used (46). These strains, which were kindly provided by Robin May, were constructed in the H99 (*C. neoformans*) and R265 (*C. gattii*) backgrounds, respectively. All strains were maintained in Sabouraud agar

plates and cultivated in Sabouraud medium at 30°C for 24 h before all experiments. RAW 264.7 macrophages were used for toxicity and phagocytosis experiments. The cells were maintained in Dulbecco's modified Eagle medium (DMEM) (catalog number D5796; Sigma-Aldrich) supplemented with 10% heat-inactivated fetal bovine serum (FBS) at 37°C in a 5% CO_2 atmosphere.

Antifungal susceptibility testing. Fenbendazole was obtained from Sigma-Aldrich (catalog number F5396) in its solid form. Stock solutions were prepared in DMSO (drug vehicle). In the antifungal susceptibility tests, vehicle concentration was kept at 1%. To determine the MIC of fenbendazole, the broth microdilution method was used following the protocols established by the European Committee on Antimicrobial Susceptibility Testing (EUCAST; E.Def 7.3.1 reference method) (47). Plates to be used in the antifungal susceptibility tests contained RPMI medium supplemented with 2% glucose buffered with 165 mM 3-(N-morpholino)propanesulfonic acid (MOPS; pH 7.0). The medium was supplemented with fenbendazole in the concentration range of 0.003 to 1.536 μg/ml. Control systems contained the drug vehicle alone. Before inoculation in the antifungal testing plates, C. neoformans and C. gattii were grown on Sabouraud agar plates at 30°C for 48 h. A suspension of 2.5×10^5 cells/ml was prepared in distilled water, and 100 μl of this suspension was transferred to each well of 96-well plates containing 100 μl of RPMI prepared as described above. The plates were incubated at 35°C for 48 h. Growth inhibition was monitored by spectrophotometric determination of optical density at 530 nm in a Molecular Devices SpectraMax Paradigm microplate reader. The MIC was defined as the lowest concentration inhibiting 90% of cryptococcal growth. Sterility control wells were included in all plates. Similar protocols were used for determination of MICs for amphotericin B, fluconazole, and benzimidazole derivatives. As recommended by EUCAST, Candida parapsilosis and Candida krusei strains (ATCC 22019 and ATCC 6258, respectively) were used as controls for the antifungal activity of amphotericin B and fluconazole. To evaluate whether fenbendazole was fungicidal or fungistatic, the cells were incubated at the MIC under the conditions described above, washed, and plated on Sabouraud agar plates and incubated for 48 h at 30°C for determination of CFU.

Checkerboard assay. The effects of the association of fenbendazole with amphotericin B on antifungal activity were evaluated using the checkerboard assay (48). The drug concentration ranges used in this assay corresponded to 0.007 to 0.5 μg/ml for amphotericin B and 0.003 to 1.536 μg/ml for fenbendazole. Drug solutions were prepared as previously described (13). Briefly, 50 μl of each of the amphotericin B concentrations was mixed with 50 μl of each of the fenbendazole solutions in microtiter plates. The vehicle concentration was 1% in all wells. Inoculation of fungal suspensions and evaluation of fungal growth followed the EUCAST protocol described in this section. The fractional inhibitory concentration index (FICI) was calculated according to the equation ΣFICI = FICI (fenbendazole) + FICI (amphotericin B), where the FICI was the ratio of the MIC of the combination with the MIC alone (49, 50). Considering the differences in chemical nature and cellular targets of fenbendazole and amphotericin B, we also calculated the Bliss synergism scores (51) against C. neoformans H99 and C. gattii R265 using the SynergyFinder tool (https://synergyfinder.fimm.fi). In this model, the scores for antagonistic drugs are lower than −10. Additive drugs produce scores in the range of −10 to 10, and synergistic drugs produce scores larger than 10.

Cytotoxicity of fenbendazole. The cytotoxicity of fenbendazole to macrophages was determined using the Cytotox 96 nonradioactive cytotoxicity assay kit (catalog number G1780; Promega) following the manufacturer's recommendations. As recently described by our group (52), macrophages were used for cell viability assays due to their fundamental roles in the control and/or dissemination of cryptococci (32). RAW 264.7 macrophages (10^5 cells/well in DMEM supplemented with 10% FBS) were treated with 0.006 to 5.98 μg/ml fenbendazole, alone or in combination with 0.06 μg/ml amphotericin B, for 24 h at 37°C in DMEM supplemented with 10% FBS. Cytotoxicity was inferred from the determination of the levels of lactate dehydrogenase activity in the medium. Control systems included vehicle-treated cells (viability control) and macrophages lysed with the lysis solution provided by the manufacturer (death control).

Effects of fenbendazole on microtubule organization. Tubulin organization in C. neoformans H99 and C. gattii R265 was evaluated as described by Wang et al. (53) with minor modifications. Briefly, fungal cells were cultivated overnight in liquid Sabouraud medium at 30°C with shaking (200 rpm). These cultures had their optical density at 600 nm (OD$_{600}$) adjusted to 0.2 in fresh Sabouraud medium and then were incubated at 30°C with shaking (200 rpm) until an OD$_{600}$ value of approximately 0.8 was reached. Samples of 1 ml of these cell suspensions were washed with PBS and resuspended in fresh Sabouraud medium supplemented with 0.12 μg/ml fenbendazole (10 times concentrated MIC value) or DMSO (0.012%). The suspensions were incubated for an additional 90 min at 30°C with shaking (200 rpm) and washed with PBS. The cells were finally suspended in 1 ml of fresh Sabouraud medium supplemented with 0.5 μl of the Tubulin Tracker green reagent (catalog number T34075; Thermo Fisher Scientific). The cells were incubated for 1 h at 37°C, washed with PBS, and fixed with 2% paraformaldehyde in PBS. Control experiments were prepared using 100 μM vinblastine (catalog number V1377; Sigma) instead of fenbendazole. Vinblastine is a tubulin-targeting alkaloid that inhibits the assembly of microtubules (54). The samples were observed under a DMi8 fluorescence microscope (Leica). Images were recorded with the LasAF software.

Effect of fenbendazole on capsular morphology. C. neoformans H99 and C. gattii R265 were grown overnight in liquid yeast extract-peptone-dextrose (YPD) medium at 30°C and washed with PBS. Yeast suspensions had their density adjusted to 5×10^4 cells/ml in a capsule induction medium (10% Sabouraud in 50 mM MOPS; pH 7.3) (55) supplemented with variable concentrations of fenbendazole. Control systems contained the vehicle alone. Capsule enlargement was induced at 37°C in a 5% CO_2 atmosphere for 0, 2, 4, 6, 8, 16, and 24 h. The cells were then washed with PBS and prepared for India

ink counterstaining after fixation with 4% paraformaldehyde and observation under a light microscope. Capsule dimensions were determined in digitalized images using the ImageJ software (56). The cells incubated for 24 h were also analyzed using other microscopic approaches. For immunofluorescence, the paraformaldehyde-fixed cells were initially blocked with 1% bovine serum albumin (BSA) in PBS for 1 h at 37°C, following staining of cell wall chitin with 25 μM calcofluor white (catalog number 18909; Sigma) in PBS for 30 min at 37°C. The cells were washed 3 times with PBS and incubated for 1 h at 37°C with a monoclonal antibody (MAb 18B7, donated by Arturo Casadevall) raised to capsular glucuronoxylomannan (GXM) at 10 μg/ml in a PBS solution containing 1% BSA. The cells were washed with PBS and incubated with an Alexa 546-antibody conjugate (catalog number A-11030; Invitrogen) recognizing mouse immunoglobulin G (1 h, 25°C in the dark). Washed cells were analyzed in a Leica SP5 AOBS laser confocal microscope. For scanning electron microscopy (SEM), the cells were washed with PBS and fixed with 2.5% glutaraldehyde in 0.1 M sodium cacodylate buffer (pH 7.2) for 1 h at 25°C. The cells were washed with a 0.1-M sodium cacodylate buffer (pH 7.2) containing 0.2 M sucrose and 2 mM $MgCl_2$. The cells were placed over 0.01% poly-L-lysine-coated coverslips and incubated for 30 min at 25°C. Adhered cells were then gradually dehydrated in ethanol (30, 50, and 70% for 5 min, and then 90% for 10 min, and 100% twice for 10 min). Immediately after dehydration, the cells were critical point dried (Leica EM CPD300), mounted on metallic bases, and coated with a gold layer (Leica EM ACE200). The cells were visualized in a scanning electron microscope (JEOL JSM-6010 Plus/LA) operating at 5 keV.

Intracellular antifungal activity. RAW 264.7 macrophages were suspended (5×10^5 cells/ml) in DMEM supplemented with 10% FBS, and 200 μl of this suspension was transferred to each well of 96-well plates for overnight incubation at 37°C in a 5% CO_2 atmosphere. The following day, *C. neoformans* H99 or *C. gattii* R265 (5×10^5 cells/ml) cells were opsonized by incubation for 1 h at 37°C under a 5% CO_2 atmosphere in DMEM containing 10% FBS and 5 μg/ml MAb 18B7. Macrophage cultures had their medium replaced with 200 μl of the above-described cell suspensions containing opsonized fungi and were incubated for 2 h (37°C, 5% CO_2). The cell cultures were washed 3 times with PBS to remove unattached fungal cells and were covered with 200 μl of DMEM containing 10% FBS, in addition to fenbendazole and/or amphotericin B (0.006 or 0.012 μg/ml fenbendazole; 0.06 or 0.5 μg/ml amphotericin B; 0.006 μg/ml fenbendazole combined with 0.06 μg/ml amphotericin B). Drug vehicle alone was used as a control. For determination of fungal killing, the drug-containing cell cultures were incubated for 24 h (37°C, 5% CO_2) and washed 3 times with PBS. The macrophages were then lysed with 200 μl of cold sterile water, and the resulting suspensions were plated on Sabouraud agar. The plates were incubated at 30°C for 48 h, and CFU were counted manually. For determination of intracellular proliferation and phagocytic escape of cryptococci, the plates containing infected macrophages were incubated at 37°C with 5% CO_2 for 18 h in an Operetta high-content imaging system (PerkinElmer). During this 18 h of incubation, images of each well were captured every 5 min with a 40$\times$ objective. Using the Harmony high-content imaging and analysis software (PerkinElmer), movies of each well were prepared for analysis of intracellular proliferation rates (IPR) and vomocytic escape (46). In each experimental condition, 50 cells were analyzed. The IPR were calculated as the t_{18}/t_0 ratio, where t_{18} is the number of fungal cells inside the macrophages after 18 h, and t_0 is the number of phagocyte-associated cryptococci at the beginning of the incubation. Vomocytosis was calculated as previously described (46) using 50 cells per experimental system. Three independent experiments were performed.

Animal experimentation. For intranasal administration of fenbendazole, C57BL/6 mice (8 to 12 weeks old) were used. The animals were kept with food and water *ad libitum* at the animal facility of the University of Brasília. The animals were placed in an isoflurane inhalation system (Bonther) for anesthesia and then challenged intratracheally with 25 μl of PBS containing 1×10^4 yeast cells of *C. neoformans* (H99 strain). After 3 days of infection, the animals were divided into groups of 5 individuals each. One group was treated intranasally with 20 μl of 1.25 μM fenbendazole. The other two groups were treated with PBS or amphotericin B (2 mg/kg) intraperitoneally as indicated in Fig. 3. Mice were fed *ad libitum* and monitored every day for discomfort and signs of disease. Mice showing weight loss, lethargy, tremor, or inability to reach food or water were euthanized, and survival was counted until that day. At day 30 any surviving mice were euthanized. Euthanasia was performed with CO_2 asphyxiation with 100% $FiCO_2$ for 2 min followed by cervical dislocation. The experiment was repeated under the same conditions, and identical results were found. All treatments and experimental procedures were performed after approval by the Ethics Committee on Animal Use (CEUA) of the University of Brasília (UnBDoc number 66729/2016) and according to the guidelines presented by the National Council for the Control of Animal Experimentation (CONCEA).

SUPPLEMENTAL MATERIAL

Supplemental material is available online only.
SUPPLEMENTAL FILE 1, PDF file, 0.1 MB.

REFERENCES

1. Bongomin F, Gago S, Oladele RO, Denning DW. 2017. Global and multi-national prevalence of fungal diseases-estimate precision. J Fungi (Basel) 3:E57.
2. Rajasingham R, Smith RM, Park BJ, Jarvis JN, Govender NP, Chiller TM, Denning DW, Loyse A, Boulware DR. 2017. Global burden of disease of HIV-associated cryptococcal meningitis: an updated analysis. Lancet Infect Dis 17:873–881. https://doi.org/10.1016/S1473-3099(17)30243-8.
3. Hurtado JC, Castillo P, Fernandes F, Navarro M, Lovane L, Casas I, Quinto L, Marco F, Jordao D, Ismail MR, Lorenzoni C, Martinez-Palhares AE, Ferreira L, Lacerda M, Monteiro W, Sanz A, Letang E, Marimon L, Jesri S, Cossa A, Mandomando I, Vila J, Bassat Q, Ordi J, Menendez C, Carrilho C, Martinez MJ. 2019. Mortality due to *Cryptococcus neoformans* and *Cryptococcus gattii* in low-income settings: an autopsy study. Sci Rep 9:7493. https://doi.org/10.1038/s41598-019-43941-w.
4. Alves Soares E, Lazera MDS, Wanke B, Faria Ferreira M, Carvalhaes de Oliveira RV, Oliveira AG, Coutinho ZF. 2019. Mortality by cryptococcosis in Brazil from 2000 to 2012: a descriptive epidemiological study. PLoS Negl Trop Dis 13:e0007569. https://doi.org/10.1371/journal.pntd.0007569.
5. Perfect JR, Dismukes WE, Dromer F, Goldman DL, Graybill JR, Hamill RJ, Harrison TS, Larsen RA, Lortholary O, Nguyen MH, Pappas PG, Powderly WG, Singh N, Sobel JD, Sorrell TC. 2010. Clinical practice guidelines for the management of cryptococcal disease: 2010 update by the infectious diseases society of america. Clin Infect Dis 50:291–322. https://doi.org/10.1086/649858.
6. Temfack E, Boyer-Chammard T, Lawrence D, Delliere S, Loyse A, Lanternier F, Alanio A, Lortholary O. 2019. New insights into *Cryptococcus* spp. biology and cryptococcal meningitis. Curr Neurol Neurosci Rep 19:81. https://doi.org/10.1007/s11910-019-0993-0.
7. Global Action Fund for Fungal Infections. 2020. Antifungal drug maps. GAFFI, Geneva, Switzerland. https://www.gaffi.org/antifungal-drug-maps/. Accessed 4 January 2020.
8. Chen T, ACTA Trial Team, Mwenge L, Lakhi S, Chanda D, Mwaba P, Molloy SF, Gheorghe A, Griffiths UK, Heyderman RS, Kanyama C, Kouanfack C, Mfinanga S, Chan AK, Temfack E, Kivuyo S, Hosseinipour MC, Lortholary O, Loyse A, Jaffar S, Harrison TS, Niessen LW, Team AT. 2019. Healthcare costs and life-years gained from treatments within the advancing cryptococcal meningitis treatment for Africa (ACTA) trial on cryptococcal meningitis: a comparison of antifungal induction strategies in sub-Saharan Africa. Clin Infect Dis 69:588–595. https://doi.org/10.1093/cid/ciy971.
9. Borba HHL, Steimbach LM, Riveros BS, Tonin FS, Ferreira VL, Bagatim BAQ, Balan G, Pontarolo R, Wiens A. 2018. Cost-effectiveness of amphotericin B formulations in the treatment of systemic fungal infections. Mycoses 61:754–763. https://doi.org/10.1111/myc.12801.
10. Chen J, Luo X, Qiu H, Mackey V, Sun L, Ouyang X. 2018. Drug discovery and drug marketing with the critical roles of modern administration. Am J Transl Res 10:4302–4312.
11. Mohs RC, Greig NH. 2017. Drug discovery and development: role of basic biological research. Alzheimers Dement (N Y) 3:651–657. https://doi.org/10.1016/j.trci.2017.10.005.
12. Krysan DJ. 2015. Toward improved anti-cryptococcal drugs: novel molecules and repurposed drugs. Fungal Genet Biol 78:93–98. https://doi.org/10.1016/j.fgb.2014.12.001.
13. de Oliveira HC, Monteiro MC, Rossi SA, Peman J, Ruiz-Gaitan A, Mendes-Giannini MJS, Mellado E, Zaragoza O. 2019. Identification of off-patent compounds that present antifungal activity against the emerging fungal pathogen *Candida auris*. Front Cell Infect Microbiol 9:83. https://doi.org/10.3389/fcimb.2019.00083.
14. Truong M, Monahan LG, Carter DA, Charles IG. 2018. Repurposing drugs to fast-track therapeutic agents for the treatment of cryptococcosis. PeerJ 6:e4761. https://doi.org/10.7717/peerj.4761.
15. McKellar QA, Scott EW. 1990. The benzimidazole anthelmintic agents: a review. J Vet Pharmacol Ther 13:223–247. https://doi.org/10.1111/j.1365-2885.1990.tb00773.x.
16. Cruz MC, Bartlett MS, Edlind TD. 1994. *In vitro* susceptibility of the opportunistic fungus *Cryptococcus neoformans* to anthelmintic benzimidazoles. Antimicrob Agents Chemother 38:378–380. https://doi.org/10.1128/AAC.38.2.378.
17. Del Poeta M, Schell WA, Dykstra CC, Jones S, Tidwell RR, Czarny A, Bajic M, Bajic M, Kumar A, Boykin D, Perfect JR. 1998. Structure-*in vitro* activity relationships of pentamidine analogues and dication-substituted bis-benzimidazoles as new antifungal agents. Antimicrob Agents Chemother 42:2495–2502. https://doi.org/10.1128/AAC.42.10.2495.
18. Del Poeta M, Schell WA, Dykstra CC, Jones SK, Tidwell RR, Kumar A, Boykin DW, Perfect JR. 1998. *In vitro* antifungal activities of a series of dication-substituted carbazoles, furans, and benzimidazoles. Antimicrob Agents Chemother 42:2503–2510. https://doi.org/10.1128/AAC.42.10.2503.
19. Nixon GL, McEntee L, Johnson A, Farrington N, Whalley S, Livermore J, Natal C, Washbourn G, Bibby J, Berry N, Lestner J, Truong M, Owen A, Lalloo D, Charles I, Hope W. 2018. Repurposing and reformulation of the antiparasitic agent flubendazole for treatment of cryptococcal meningoencephalitis, a neglected fungal disease. Antimicrob Agents Chemother 62:e01909-17. https://doi.org/10.1128/AAC.01909-17.
20. Joffe LS, Schneider R, Lopes W, Azevedo R, Staats CC, Kmetzsch L, Schrank A, Del Poeta M, Vainstein MH, Rodrigues ML. 2017. The Anti-helminthic compound mebendazole has multiple antifungal effects against *Cryptococcus neoformans*. Front Microbiol 8:535.
21. CVMP. 2014. CVMP assessment report for Panacur AquaSol (EMEA/V/C/002008/X/0003)—international non-proprietary name: fenbendazole.

(CVMP) CfMPfVU. European Medicines Agency, London, United Kingdom.

22. Villar D, Cray C, Zaias J, Altman NH. 2007. Biologic effects of fenbendazole in rats and mice: a review. J Am Assoc Lab Anim Sci 46:8–15.

23. Ianevski A, He L, Aittokallio T, Tang J. 2017. SynergyFinder: a web application for analyzing drug combination dose-response matrix data. Bioinformatics 33:2413–2415. https://doi.org/10.1093/bioinformatics/btx162.

24. Lacey E. 1988. The role of the cytoskeletal protein, tubulin, in the mode of action and mechanism of drug resistance to benzimidazoles. Int J Parasitol 18:885–936. https://doi.org/10.1016/0020-7519(88)90175-0.

25. Furtado LFV, de Paiva Bello ACP, Rabelo E. 2016. Benzimidazole resistance in helminths: from problem to diagnosis. Acta Trop 162:95–102. https://doi.org/10.1016/j.actatropica.2016.06.021.

26. Kopecka M. 2016. Microtubules and actin cytoskeleton of *Cryptococcus neoformans* as targets for anticancer agents to potentiate a novel approach for new antifungals. Chemotherapy 61:117–121. https://doi.org/10.1159/000437134.

27. Gottschall DW, Theodorides VJ, Wang R. 1990. The metabolism of benzimidazole anthelmintics. Parasitol Today 6:115–124. https://doi.org/10.1016/0169-4758(90)90228-V.

28. Johnston SA, May RC. 2013. *Cryptococcus* interactions with macrophages: evasion and manipulation of the phagosome by a fungal pathogen. Cell Microbiol 15:403–411. https://doi.org/10.1111/cmi.12067.

29. Casadevall A, Coelho C, Cordero RJB, Dragotakes Q, Jung E, Vij R, Wear MP. 2019. The capsule of *Cryptococcus neoformans*. Virulence 10:822–831. https://doi.org/10.1080/21505594.2018.1431087.

30. Bojarczuk A, Miller KA, Hotham R, Lewis A, Ogryzko NV, Kamuyango AA, Frost H, Gibson RH, Stillman E, May RC, Renshaw SA, Johnston SA. 2016. *Cryptococcus neoformans* intracellular proliferation and capsule size determines early macrophage control of infection. Sci Rep 6:21489. https://doi.org/10.1038/srep21489.

31. Alanio A, Desnos-Ollivier M, Dromer F. 2011. Dynamics of *Cryptococcus neoformans*: macrophage interactions reveal that fungal background influences outcome during cryptococcal meningoencephalitis in humans. mBio 2. https://doi.org/10.1128/mBio.00158-11.

32. Garcia-Rodas R, Zaragoza O. 2012. Catch me if you can: phagocytosis and killing avoidance by *Cryptococcus neoformans*. FEMS Immunol Med Microbiol 64:147–161. https://doi.org/10.1111/j.1574-695X.2011.00871.x.

33. Seoane PI, May RC. 2020. Vomocytosis: what we know so far. Cell Microbiol 22:e13145.

34. Alvarez M, Casadevall A. 2006. Phagosome extrusion and host-cell survival after *Cryptococcus neoformans* phagocytosis by macrophages. Curr Biol 16:2161–2165. https://doi.org/10.1016/j.cub.2006.09.061.

35. Menotti J, Alanio A, Sturny-Leclere A, Vitry S, Sauvage F, Barratt G, Bretagne S. 2017. A cell impedance-based real-time *in vitro* assay to assess the toxicity of amphotericin B formulations. Toxicol Appl Pharmacol 334:18–23. https://doi.org/10.1016/j.taap.2017.08.017.

36. Reis FCG, Borges BS, Jozefowicz LJ, Sena BAG, Garcia AWA, Medeiros LC, Martins ST, Honorato L, Schrank A, Vainstein MH, Kmetzsch L, Nimrichter L, Alves LR, Staats CC, Rodrigues ML. 2019. A novel protocol for the isolation of fungal extracellular vesicles reveals the participation of a putative scramblase in polysaccharide export and capsule construction in *Cryptococcus gattii*. mSphere 4:e00080-19. https://doi.org/10.1128/mSphere.00080-19.

37. Page SW. 2008. Antiparasitic drugs, p 584. *In* Maddison JE, Page SW, Church DB (ed), Small animal clinical pharmacology. Elsevier, Philadelphia, PA. https://doi.org/10.1016/B978-0-7020-2858-8.X5001-5.

38. Cruz MC, Edlind T. 1997. beta-Tubulin genes and the basis for benzimidazole sensitivity of the opportunistic fungus *Cryptococcus neoformans*. Microbiology 143:2003–2008. https://doi.org/10.1099/00221287-143-6-2003.

39. Petersen MB, Friis C. 2000. Pharmacokinetics of fenbendazole following intravenous and oral administration to pigs. Am J Vet Res 61:573–576. https://doi.org/10.2460/ajvr.2000.61.573.

40. Crowe TP, Greenlee MHW, Kanthasamy AG, Hsu WH. 2018. Mechanism of intranasal drug delivery directly to the brain. Life Sci 195:44–52. https://doi.org/10.1016/j.lfs.2017.12.025.

41. Haschke M, Suter K, Hofmann S, Witschi R, Frohlich J, Imanidis G, Drewe J, Briellmann TA, Dussy FE, Krahenbuhl S, Surber C. 2010. Pharmacokinetics and pharmacodynamics of nasally delivered midazolam. Br J Clin Pharmacol 69:607–616. https://doi.org/10.1111/j.1365-2125.2010.03611.x.

42. Bruinsmann FA, Richter Vaz G, de Cristo Soares Alves A, Aguirre T, Raffin Pohlmann A, Stanisçuaski Guterres S, Sonvico F. 2019. Nasal drug delivery of anticancer drugs for the treatment of glioblastoma: preclinical and clinical trials. Molecules 24:4312. https://doi.org/10.3390/molecules24234312.

43. Zhang Z, Tang W. 2018. Drug metabolism in drug discovery and development. Acta Pharm Sin B 8:721–732. https://doi.org/10.1016/j.apsb.2018.04.003.

44. Sabiiti W, Robertson E, Beale MA, Johnston SA, Brouwer AE, Loyse A, Jarvis JN, Gilbert AS, Fisher MC, Harrison TS, May RC, Bicanic T. 2014. Efficient phagocytosis and laccase activity affect the outcome of HIV-associated cryptococcosis. J Clin Invest 124:2000–2008. https://doi.org/10.1172/JCI72950.

45. Montresor A, Gabrielli AF, Diarra A, Engels D. 2010. Estimation of the cost of large-scale school deworming programmes with benzimidazoles. Trans R Soc Trop Med Hyg 104:129–132. https://doi.org/10.1016/j.trstmh.2009.10.007.

46. Voelz K, Johnston SA, Rutherford JC, May RC. 2010. Automated analysis of cryptococcal macrophage parasitism using GFP-tagged cryptococci. PLoS One 5:e15968. https://doi.org/10.1371/journal.pone.0015968.

47. Arendrup MC, Meletiadis J, Mouton JW, Guinea J, Cuenca-Estrella M, Lagrou K, Howard SJ, Subcommittee on Antifungal Susceptibility Testing of the EECfAST. 2016. EUCAST technical note on isavuconazole breakpoints for *Aspergillus*, itraconazole breakpoints for *Candida* and updates for the antifungal susceptibility testing method documents. Clin Microbiol Infect 22:571.e1-4. https://doi.org/10.1016/j.cmi.2016.01.017.

48. Rossi SA, de Oliveira HC, Agreda-Mellon D, Lucio J, Mendes-Giannini MJS, García-Cambero JP, Zaragoza O. 2020. Identification of off-patent drugs that show synergism with amphotericin B or that present antifungal action against *Cryptococcus neoformans* and *Candida* spp. Antimicrob Agents Chemother 64:e01921-19. https://doi.org/10.1128/AAC.01921-19.

49. Meletiadis J, Pournaras S, Roilides E, Walsh TJ. 2010. Defining fractional inhibitory concentration index cutoffs for additive interactions based on self-drug additive combinations, Monte Carlo simulation analysis, and *in vitro-in vivo* correlation data for antifungal drug combinations against *Aspergillus fumigatus*. Antimicrob Agents Chemother 54:602–609. https://doi.org/10.1128/AAC.00999-09.

50. Odds FC. 2003. Synergy, antagonism, and what the chequerboard puts between them. J Antimicrob Chemother 52:1–1. https://doi.org/10.1093/jac/dkg301.

51. Zhao W, Sachsenmeier K, Zhang L, Sult E, Hollingsworth RE, Yang H. 2014. A new Bliss independence model to analyze drug combination data. J Biomol Screen 19:817–821. https://doi.org/10.1177/1087057114521867.

52. Silva VKA, May RC, Rodrigues ML. 2020. Pyrifenox, an ergosterol inhibitor, differentially affects *Cryptococcus neoformans* and *Cryptococcus gattii*. Med Mycol https://doi.org/10.1093/mmy/myz132.

53. Wang LL, Lee KT, Jung KW, Lee DG, Bahn YS. 2018. The novel microtubule-associated CAP-glycine protein Cgp1 governs growth, differentiation, and virulence of *Cryptococcus neoformans*. Virulence 9:566–584. https://doi.org/10.1080/21505594.2017.1423189.

54. Gigant B, Wang C, Ravelli RB, Roussi F, Steinmetz MO, Curmi PA, Sobel A, Knossow M. 2005. Structural basis for the regulation of tubulin by vinblastine. Nature 435:519–522. https://doi.org/10.1038/nature03566.

55. Zaragoza O, Casadevall A. 2004. Experimental modulation of capsule size in *Cryptococcus neoformans*. Biol Proced Online 6:10–15. https://doi.org/10.1251/bpo68.

56. Schneider CA, Rasband WS, Eliceiri KW. 2012. NIH Image to ImageJ: 25 years of image analysis. Nat Methods 9:671–675. https://doi.org/10.1038/nmeth.2089.